Medicinal Chemistry Research (2024) 33:1229–1241
https://doi.org/10.1007/s00044-024-03256-6

MEDICINAL CHEMISTRY RESEARCH

ORIGINAL RESEARCH ARTICLE

N-Benzyl, *N*-phenethyl and *N*-benzyloxybenzamide derivatives inhibit amyloid-beta (Aβ42) aggregation and mitigate Aβ42-induced neurotoxicity

Yusheng Zhao[1] · Arash Shakeri[1] · Ahmed A. Hefny[1] · Praveen P. N. Rao[1]

Received: 8 December 2023 / Accepted: 5 June 2024 / Published online: 15 June 2024
© The Author(s), under exclusive licence to Springer Science+Business Media, LLC, part of Springer Nature 2024

Abstract

A library of *N*-benzylbenzamide, *N*-phenethylbenzamide and *N*-benzyloxybenzamide derivatives were designed, synthesized and evaluated as amyloid beta (Aβ42) aggregation inhibitors. These compounds were designed by replacing the α,β-unsaturated linker region of chalcone with an amide bioisostere. The Aβ42 aggregation inhibition properties of these 27 benzamide derivatives were evaluated by the thioflavin T (ThT)-based fluorescence aggregation kinetics assay, transmission electron microscopy (TEM) studies, Aβ42-induced cytotoxicity assay in mouse hippocampal neuronal HT22 cell lines, fluorescence live cell imaging, and computational modelling studies using a pentamer model of Aβ42. These studies led to the identification of *N*-benzylbenzamides **3a** and **3f**, *N*-phenethylbenzamide **5a** and *N*-benzyloxybenzamide **7a** as promising compounds that were able to exhibit anti-aggregation properties in the ThT-based fluorescence experiments, TEM studies and more significantly were able to rescue the hippocampal neuronal HT22 cells from Aβ42-induced cytotoxicity (91–96% cell viability at 25 μM). These results demonstrate the usefulness of these benzamide-based templates in the design and development of novel small molecules as chemical tools and therapeutics to study and treat Alzheimer's disease.

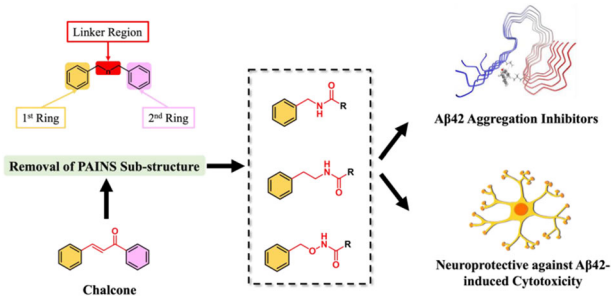

Keywords Chalcone · PAINS · Benzamide derivatives · Aβ42 aggregation · TEM · Cytotoxicity · HT22 cell line · Molecular docking

Introduction

Alzheimer's disease (AD) is the most common type of dementia. With an increase in the aging population worldwide, the incidence and prevalence of AD are predicted to rise in the coming years. AD is a neurodegenerative disorder that significantly hampers the function of the central nervous system, especially the brain regions of learning and memory [1–4]. Unfortunately, the diverse, complex, yet unified neurodegenerative pathophysiological pathways, have stalled the discovery of novel drug candidates to treat and cure AD. One of the known factors of AD is the aggregation of amyloid-beta (Aβ) peptides into neurotoxic forms [4, 5]. Recent evidence have shown that Aβ aggregation can trigger other AD pathological pathways either directly or indirectly to promote

✉ Praveen P. N. Rao
praveen.nekkar@uwaterloo.ca

[1] School of Pharmacy, Health Sciences Campus, University of Waterloo, 200 University Avenue Wes, Waterloo, ON N2L 3G1, Canada

neurodegeneration and cognitive decline [6–9]. The Aβ peptide formed after the proteolytic degradation of the amyloid precursor protein, undergoes rapid self-assembly and aggregation to form the senile plaques found in AD patient brain [4, 5, 10]. Based on these findings, the inhibition of Aβ aggregation would provide therapeutic benefits to AD patients. Recent years saw an uptick in the discovery and development of novel anti-Aβ therapies as a novel class of disease-modifying agents to treat AD [11, 12]. In this regard, two monoclonal antibodies: aducanumab (Aduhelm®) and lecanemab (Leqembi®) received approval from the US Food and Drug Administration with the later receiving full approval recently. Another monoclonal antibody, donanemab, is poised to receive FDA approval soon [13–16]. These developments in the AD drug discovery field demonstrate that targeting the amyloid cascade holds promise as a strategy to treat AD.

The field is now ripe to discover and develop novel anti-Aβ therapies based on small molecules since they are less expensive to manufacture, exhibit better stability on storage and can be administered orally which is beneficial to AD patients [17]. In this regard, we are working on designing novel small molecules that can bind to Aβ and prevent its aggregation into toxic forms [18–20]. We focused our attention on the small molecule chalcone (**1**) considered as privileged structure (Fig. 1) and is known to demonstrate anti-aggregation properties toward Aβ [21–26]. However, chalcone has been identified as pan-assay interfering compound (PAINS) [25–30]. They interact with their molecular targets and biological thiols with no specificity, thus providing false positives and interfere with either UV- or fluorescence-based screening assays. The presence of the α,β-unsaturated system in their chemical structure makes them function as Michael acceptors, and the chalcone template can undergo covalent bonding with biological thiols [25, 26, 30]. Therefore, small molecules with these templates are flagged as PAINS in drug development. However, these still represent privileged structures in medicinal chemistry that can be optimized to design and develop novel agents. In this regard, previous studies have demonstrated that molecules bearing flat and planar C_6-C_n-C_6 carbon chain template are favoured to bind and prevent Aβ self-assembly (Fig. 1), where C_6 refers to the presence of two aromatic rings and C_n refers to the type of linkage present between two aromatic ring systems [31].

Based on these findings, we adopted the C_6-C_n-C_6 template and replaced the Michael acceptor α,β-unsaturated system with an amide bioisostere to obtain the benzamide template (Fig. 1). This template has the following advantages: i) amide bond is not considered as PAINS [30] and does not undergo Michael addition with biological molecules; ii) the resonance delocalization in amide bond provides double bond characteristic and can act as a bioisostere of the α,β-unsaturated system present in chalcone. Thus, the flexibility of the designed ligands would be comparable to chalcone which fulfils the requirements to bind and prevent Aβ aggregation; iii) furthermore, from a synthetic chemistry point of view, amide bond eliminates the need to evaluate *cis/trans* or (*Z*)-/(*E*) isomers. Based on these hypotheses, we synthesized a library of 27 *N*-benzyl, *N*-phenethyl and *N*-benzyloxybenzamide derivatives, with various aromatic substituents and linkers containing either carbon spacer (**3a–i** and **5a–i**), or oxygen spacer (**7a–i**). Their bioactivity toward Aβ42 aggregation was investigated by carrying out thioflavin T (ThT) fluorescence-based aggregation kinetic study, transmission electron microscopy (TEM), computational modelling and cell viability studies in mouse hippocampal HT22 neuronal cell lines against Aβ42 induced cytotoxicity. These studies demonstrate that the benzamide derivatives exhibit anti-Aβ42 activity in the thioflavin T (ThT) based fluorescent spectroscopy and electron microscopy experiments. Strikingly, these compounds demonstrate excellent neuroprotection against Aβ42-induced neurotoxicity in HT22 mouse hippocampal neuronal cells.

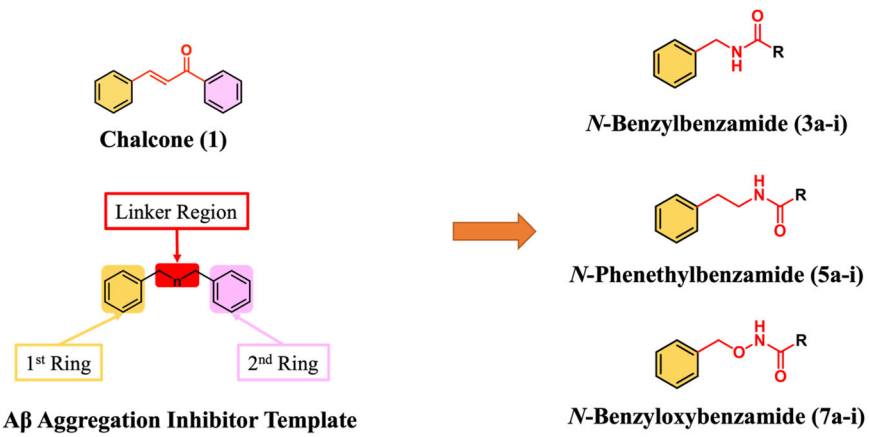

Fig. 1 Designing amide-linked benzamide derivatives based on the known Aβ aggregation inhibitor chalcone. The α,β-unsaturated system was replaced by an amide bioisostere. The aromatic rings (yellow, 1st ring; pink, 2nd ring), and the linker regions (red) are color-coded

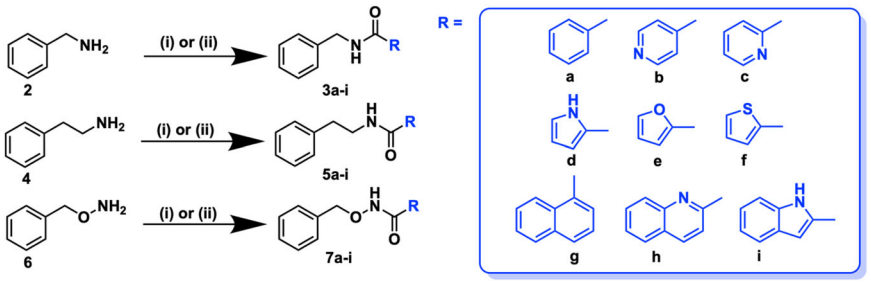

Scheme. 1 Synthetic scheme to prepare **3a–i, 5a–i**, and **7a–i**. Reagents and conditions: (i) TEA, acid chlorides (RCOCl), THF, room temperature/reflux 6–24 h. (ii) carboxylic acids (R-COOH), TEA, EDC•HCl, HOBt, THF, room temperature overnight

Results and discussion

Chemistry

The synthesis of target benzamide derivatives (27 compounds), was accomplished through direct coupling of primary amines (phenylmethanamine **2**, or 2-phenylethan-1-amine **4**, or *O*-benzylhydroxylamine **6**) with the corresponding acid chlorides (RCOCl) using triethylamine (TEA) either at room temperature or under reflux using known chemistry (Scheme 1). Alternatively, the benzamide derivatives were synthesized by coupling the corresponding acids (RCOOH) with primary amines using standard amide coupling agent EDC•HCl and HOBt in the presence of TEA (Scheme 1) [32, 33]. The target compounds **3a–i, 5a–i** and **7a–i** were obtained in good-to-excellent yields ranging from 72–93%. Coupling the acids with amines generally provided greater yields. Analytical data of final compounds **3a–i, 5a–i** and **7a–i** is provided in the Supplementary Material file.

Biological activity studies

Evaluation of the anti-Aβ42 aggregation activity of 3a–i, 5a–i and 7a–i in the thioflavin T (ThT) based fluorescence spectroscopy

The structure-activity relationship (SAR) of benzamide derivatives to inhibit Aβ42 aggregation was evaluated by ThT-based fluorescence kinetic assay [19]. The benzamide derivatives **3a–i, 5a–i** and **7a–i** (25 µM) were incubated with Aβ42 (10 µM) at 37 °C, pH 7.4 and the ThT fluorescence intensity was measured after 24 h incubation period to determine the anti-aggregation activity. The results are summarized in Fig. 2. In the *N*-benzylbenzamide series (**3a–i**), the presence of an unsubstituted benzene ring in compound **3a** (R=benzene) provided 27.1 ± 2.3% inhibition of Aβ42 aggregation (Fig. 2). Replacing the benzene ring with the corresponding pyridine bioisostere in compounds **3b** and **3c**, led to a significant reduction in their anti-aggregation activity (~ 19% and 13% inhibition, Fig. 2). In contrast, incorporating five-member heterocycles (eg: pyrrole, furan and thiophene) restored the anti-Aβ42 activity with compounds **3d, 3e** and **3 f** exhibiting 23.8–27.8% inhibition range (Fig. 2). The SAR was further investigated by incorporating planar, bicyclic aromatic rings (eg: naphthyl, quinoline and indole). These changes led to mixed results with compound **3 h** (R=quinoline), demonstrating comparable inhibition (~ 27%, Fig. 2), similar to compound **3a** (R=benzene, 27% inhibition, Fig. 2). Incorporating the planar, bicyclic indole ring led to a significant loss of anti-aggregation activity in compound **3i** (~7% inhibition of Aβ42 aggregation, Fig. 2), whereas the presence of a naphthyl ring in compound **3 g**, provided moderate inhibition (~ 16%, Fig. 2). In the *N*-phenethylbenzamide series (**5a–i**), the addition of an extra carbon spacer did not change their ability to prevent Aβ42 aggregation (Fig. 2) and similar pattern was seen. In this series, compound **5a** (R = benzene, ~ 28% inhibition, Fig. 2), was identified as the best with comparable activity as **3a** (~27% inhibition). The next best compound was **5 f** possessing a five-member thiophene ring (~ 27% inhibition, Fig. 2). Similar to the *N*-benzylbenzamide series, the addition of a planar, bicyclic indole ring led to a significant loss in the Aβ42 inhibition activity (**5i**, ~ 7% inhibition, Fig. 2). In the *N*-benzyloxybenzamide series (**7a–i**), the SAR was investigated by adding an oxygen linker next to the amide nitrogen. In this series, compound **7a** (R=benzene, 26% inhibition) was identified as the best compound, followed by compounds **7i, 7f, 7d** and **7 g** with activity ranging from 23–25% (Fig. 2). These studies demonstrate that the *N*-benzyl, *N*-phenethyl and *N*-benzyloxybenzamide derivatives have the potential to be developed as Aβ42 aggregation inhibitors.

Transmission electron microscopy studies of 3a, 3f, 3h, 5a, 5f and 7a in the presence of Aβ42

Next, we investigated the Aβ42 aggregation inhibition properties of representative benzamide derivatives (**3a, 3f, 3h, 5a, 5f** and **7a**, Fig. 3) by carrying out transmission electron microscopy (TEM) experiments [19]. The morphology of Aβ42 (10 µM) shows a combination of long, twisted, unbranched mature fibrils. In the presence of

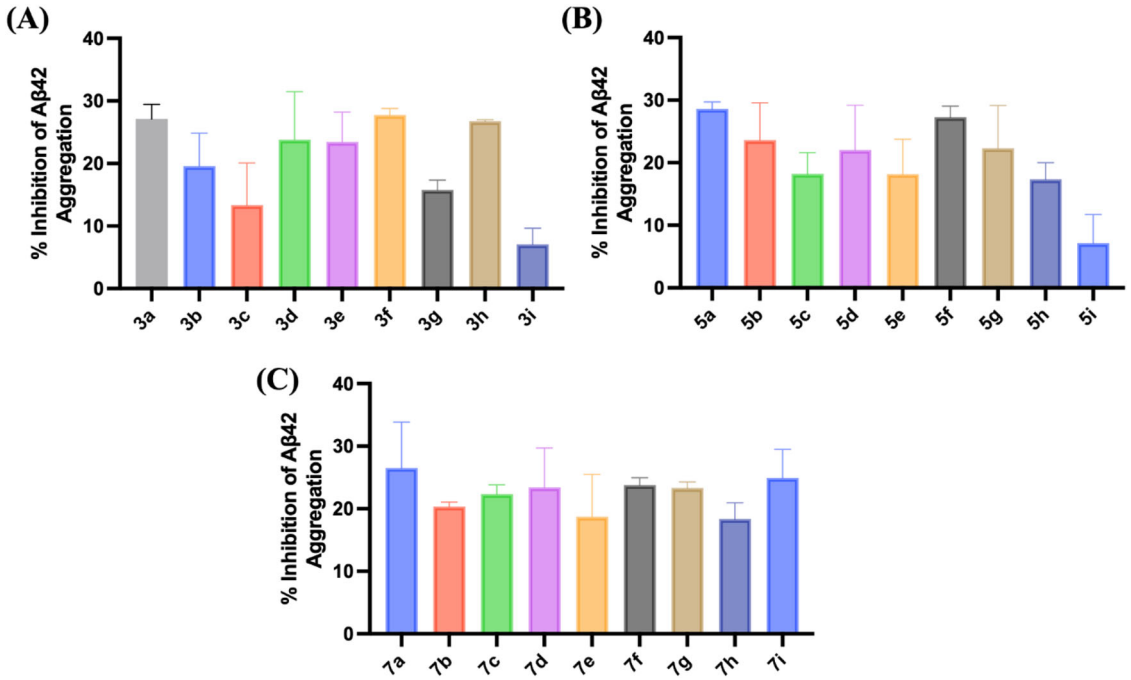

Fig. 2 Inhibition activity of benzamide derivatives (**3a–i, 5a–i** and **7a–i**, 25 μM each) against Aβ42 aggregation at 24 h time period. The compounds (25 μM) were incubated with Aβ42 (10 μM) for 24 h at 37 °C, pH 7.4 and the ThT fluorescence was monitored (excitation=440 nm, emission=490 nm). The results shown are average±standard deviation of triplicate readings based on three independent experiments

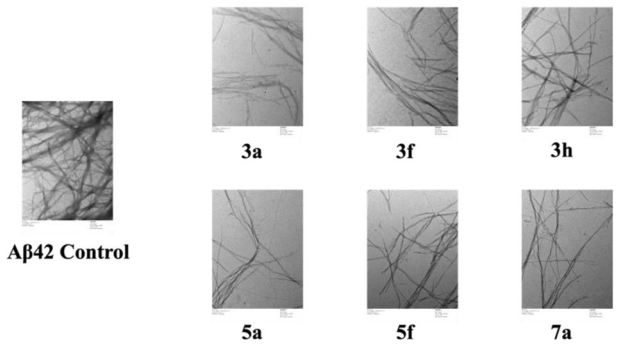

Fig. 3 TEM images of Aβ42 (10 μM) in the presence and absence of benzamide derivatives (25 μM). Scale: 200 μm

benzamide derivatives, there was a significant reduction in the formation of Aβ42 fibrils which was characterized by the presence of sparse, thinner, and lower-ordered fibrils (Fig. 3). TEM studies further demonstrate the Aβ42 aggregation inhibition potential of these benzamides.

Effect of 3a, 3f, 3h, 5a, 5f, and 7a on Aβ42-induced cytotoxicity in mouse hippocampal HT22 neuronal cells

In order to determine if the benzamide derivatives were capable of modifying the Aβ42 aggregation pathway in cellular environment, we investigated the ability of representative benzamide derivatives to prevent Aβ42-mediated cytotoxicity in mouse hippocampal HT22 neuronal cell lines. The cytotoxicity of benzamide derivatives (**3a, 3f, 3h, 5a, 5f**, and **7a**) alone, was evaluated in HT22 cells using the cell counting kit 8 (CCK-8)-based colorimetric assay [34]. These studies show that at 25 μM, these benzamide derivatives were not toxic to cells (83–110% viability) compared to untreated cells (UC) as shown in Fig. 4A. Then, HT22 cells were incubated with Aβ42 (5 μM) in the presence and absence of benzamide derivatives (25 μM) for 48 h. The cell viability reduced dramatically in the presence of Aβ42 (~ 39%, Fig. 4B). In contrast, benzamides **3a, 3f, 3h, 5a, 5f**, and **7a** demonstrated significant neuroprotection to HT22 cells against Aβ42-induced neurotoxicity, and demonstrated cell viability ranging from 81–97% (Fig. 4B). For example, benzamides **3a** (R=benzene), **3f** (R=thiophene), **5a** (R=benzene), and **7a** (R=benzene) exhibited excellent neuroprotection against Aβ42-induced neurotoxicity (94.9 ± 5.9%, 95.9 ± 13.7%, 96.7 ± 14.9%, and 91.5 ± 8.3% cell viability respectively). These striking neuroprotection observed suggests that benzamide derivatives have the potential to convert toxic Aβ assemblies into nontoxic forms thereby reducing the cytotoxic effects of Aβ42 assemblies [34]. This provides further evidence that *N*-benzyl, *N*-phenethyl and *N*-benzyloxybenzamides are novel templates that can be employed by researchers to design and discover anti-AD agents.

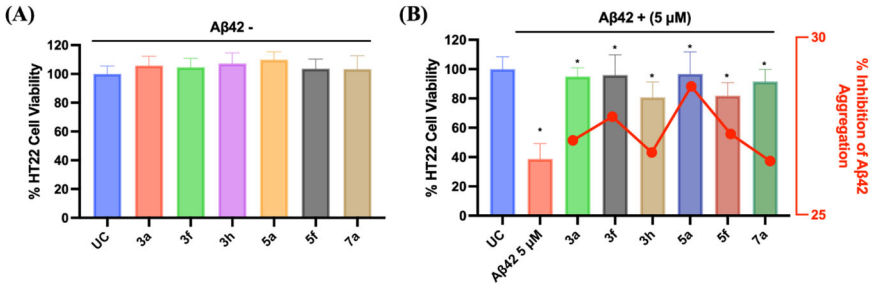

Fig. 4 Neuroprotective effect of benzamides **3a, 3d, 3f, 5a, 5 f, 7a** on HT22 hippocampal cells. Panel **A** (cell viability on y-axis) shows the effect of compounds alone (25 μM each) on HT22 hippocampal neuronal cells after 48 h incubation and Panel **B** shows the effect of compounds (25 μM each) on HT22 cells treated with Aβ42 (5 μM) after 48 h incubation. Cell viability was determined by CCK-8 based colorimetric assay. The cell viability data in Panel **B** (left y-axis) was correlated with the Aβ42 aggregation percent inhibition of compounds obtained from the ThT assay (right y-axis). The results shown are average of quadruplicate readings based on three independent experiments. $*p < 0.01$ compared to Aβ42-treated group (One-way ANOVA followed by Bonferroni post hoc test)

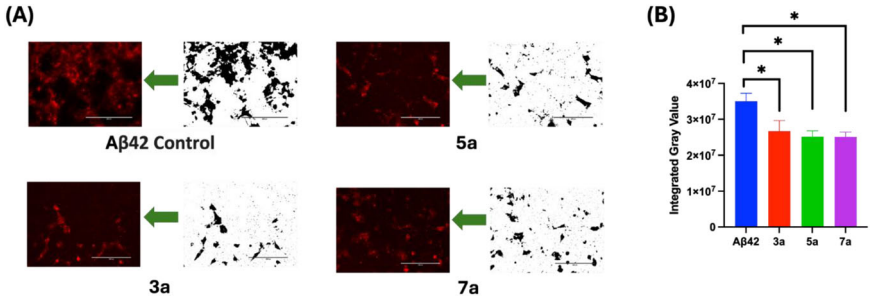

Fig. 5 Fluorescence live cell imaging with ProteoStat®. **A** Images of HT22 cells treated with Aβ42 (10 μM) in the presence and absence of compounds **3a, 5a**, and **7a** at 25 μM. The images were visualized with the RFP light filter and the binary masks were created to measure the integrated gray value (IGV) of the original fluorescence images. **B** Quantitative analysis of ProteoStat® measured by IGV in the presence and absence of compounds **3a, 5a**, and **7a**. The results shown are averages of three independent experiments from three randomized views. $*p < 0.01$ compared to the Aβ42 control group (One-way ANOVA followed by Bonferroni post hoc test)

ProteoStat® based fluorescence imaging studies in mouse hippocampal (HT22) neuronal cells

To further validate the anti-aggregation activities of compounds **3a, 5a**, and **7a** in the cellular environment, live cell fluorescence imaging studies were carried out. The dye ProteoStat® which selectively stains amyloidogenic protein aggregates [35] was used to quantitatively measure and visualize the formation of Aβ42 fibrils in the mouse hippocampal HT22 cell lines in the presence and absence of compounds **3a, 5a**, and **7a** (25 μM each). When the cells were exposed to Aβ42 alone or the presence of test compounds, the presence of mature β sheet-rich structures was marked by the red ProteoStat® stain (Fig. 5A). The stain density was quantified by summing up the pixel values as the integrated gray value (IGV) using the software ImageJ. These studies show that there was a clear decrease in the amount of Aβ42 fibrils formed in the presence of derivatives **3a, 5a**, and **7a** (Fig. 5B). The highest IGV was observed for the Aβ42 control group, with a value of 3.5×10^7 (Fig. 5B). When the cells were co-incubated with aggregation inhibitors **3a, 5a**, and **7a**, there was a reduction in the IGV which demonstrates the ability of these compounds to reduce the formation of Aβ42 fibrils. For compound **3a**, around 24% decrease in IGV (2.67×10^7) was observed whereas for compounds **5a** and **7a**, around 28% and 29% decreases in Aβ42 fibril density was observed which further provides evidence on their ability to inhibit the aggregation of Aβ42 in the cellular environment.

LDH release cytotoxicity assay in mouse hippocampal HT22 neuronal cells

One of the mechanisms of Aβ42 cytotoxicity is related to its ability to interact with the lipid membrane which leads to the formation of pores and eventual cell lysis [36]. In this regard, the ability of compounds **3a, 5a**, and **7a** to rescue the HT22 cells from Aβ42-induced neurotoxicity was evaluated by the lactate dehydrogenase (LDH) assay. Cell membranes can become damaged and leaky due to Aβ42-induced toxicity and consequently, cytosolic LDH can get released which can be measured to determine cytotoxicity [37]. Our studies show that the exposure of Aβ42 to HT22 cell lines led to a 1.29-fold increase in the LDH release compared to untreated cells

(Fig. 6), indicating that Aβ42 can cause damage to cell membranes. When the cells were co-incubated with Aβ42 and compounds **3a, 5a**, and **7a** (25 µM each), the amount of LDH released was reduced significantly (to 0.93, 0.98, and 1.04-fold respectively for compounds **3a, 5a** and **7a** as shown in Fig. 6). These results further provide evidence that *N*-benzyl, *N*-phenethyl and *N*-benzyloxybenzamides are able to protect HT22 cells from Aβ42-induced cytotoxicity.

In silico physicochemical and ADME analysis

The physiochemical properties, blood-brain barrier (BBB) penetration and presence of structural alerts were predicted for representative compounds **3a, 3f, 5a** and **7a** using the web tool SwissADME [38]. These results show that benzamide derivatives demonstrate drug-like properties with Log P values ranging from 2.28–2.93, and are predicted to cross into BBB, without the liability of possessing any structural alerts (Table 1).

Molecular docking studies of 3a, 5a and 7a in the Aβ42 pentamer model

The binding interactions of benzamide derivatives from each series (**3a, 5a**, and **7a**), were investigated in the Aβ42 pentamer assembly by carrying out molecular docking studies [34]. The Aβ42 pentamer model was prepared using the solved 3D structure of Aβ42 fibril (PDB: 5KK3) [39]. The two regions of Aβ42, the KLVFFA and the C-terminal IGLMVGGVVIA hydrophobic tail region are of great interest due to their role in the self-assembly process. Molecular docking studies show that the benzamide derivatives (**3a, 5a** and **7a**) were able to interact with both the KLVFFA and IGLMVGGVVIA regions (Fig. 7). The ribbon diagram of **3a, 5a** and **7a** docked to Aβ42 pentamer in Fig. 7A and the 2D interaction maps are shown in Fig. 7B, C. It is interesting to note that all three derivatives exhibited similar binding modes and were in the same binding region between the C- and N-termini (Fig. 7). The aromatic rings at either ends underwent hydrophobic and van der Waal's interactions with Leu17 and Leu34 (distance ~ 5.0 Å) respectively. This study also shows that the aromatic rings were the major contributor to their interactions with the C- and N-termini regions of Aβ42. Furthermore, the linker regions in **3a, 5a** and **7a** also underwent van der Waal's interactions with Gln15, Leu17 and Leu34 amino acid residues (distance ~ 5.0 Å). This suggests that the *N*-benzylbenzamide, *N*-phenethylbenzamide and *N*-benzyloxybenzamide templates can undergo hydrophobic and van der Waal's contact with the Leu17 and Leu34 to stabilize the conformation and prevent further aggregation. The CDOCKER energy and the CDOCKER interaction energies for **3a, 5a** and **7a** are given in (Table 2) which shows that they all form stable complexes with the Aβ42 pentamer.

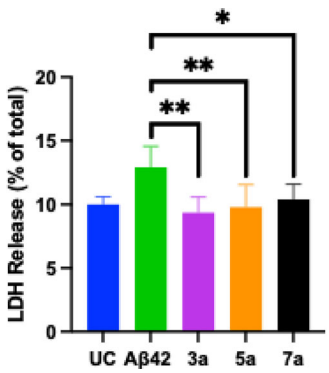

Fig. 6 Percentage LDH release from HT22 cell lines when exposed to Aβ42 (10 µM) in the presence and absence of lead derivatives **3a, 5a**, and **7a** at 25 µM. The results shown are averages of quadruplicate readings based on three independent experiments. *$p < 0.001$ compared to the Aβ42 control group; **$p < 0.0001$ compared to the Aβ42 control group (One-way ANOVA followed by Bonferroni post hoc test)

Conclusion

In summary, we designed a library of 27 small molecules by replacing the α,β-unsaturated system present in the chalcone template with an amide bioisostere to obtain benzamide derivatives and evaluated them as inhibitors of Aβ42 aggregation. These derivatives possess either *N*-benzylbenzamide, *N*-phenethylbenzamide or *N*-benzyloxybenzamide templates. The ThT-based anti-aggregation studies show that the compounds **3a, 3f, 3h, 5a, 6f** and **8a** exhibit ~ 27–28% inhibition of Aβ42 aggregation. Their

Table. 1 Predicted physicochemical, BBB permeation, and structural alerts for **3a, 3f, 5a**, and **7a** using the web tool SwissADME

Compound	MW	H-Bond Acceptor	H-Bond Donor	TPSA Å^2	BBB Permeability	Consensus LogP	Structural alert
3a	211.26	1	1	29.1	Yes	2.6	0
3f	217.29	1	1	57.3	Yes	2.62	0
5a	225.29	1	1	29.1	Yes	2.93	0
7a	227.26	2	1	38.3	Yes	2.28	0
Chalcone	208.26	1	0	17.0	Yes	3.25	1 (Michael acceptor)

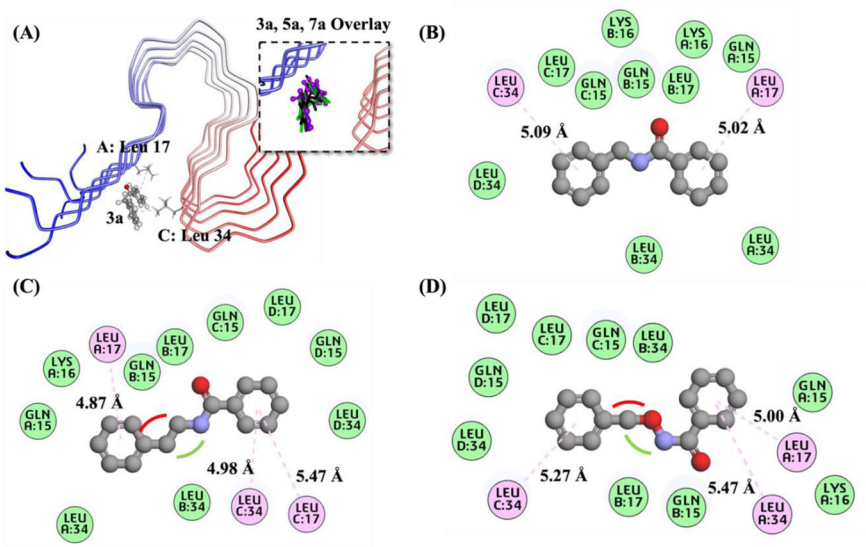

Fig. 7 Binding modes of **3a, 5a** and **7a** in the Aβ42 pentamer model (PDB: 5KK3). **A** The binding mode of **3a** in the Aβ42 pentamer model (red and blue regions highlighting the C- and N-termini), and close-up view of **3a** (purple), **5a** (black), and **7a** (green) bound to the pentamer assembly. **B–D** 2D interaction map of **3a, 5a**, and **7a**. The atoms are color-coded (carbon in grey, nitrogen in blue, and oxygen in red). The hydrophobic interactions are shown in pink and the van der Waals interactions are shown in green. The hydrogen atoms were removed to enhance clarity

Table. 2 Benzamide-Aβ42 pentamer complex energy parameters obtained after molecular docking study of **3a, 5a**, and **7a**

Cmpd	CDOCKER Energy (kcal/mol)[a]	CDOCKER Interaction Energy (kcal/mol)[a]
3a	− 18.83	− 23.76
5a	− 21.78	− 26.50
7a	− 17.42	− 23.17

[a]The energy terms CDOCKER energy and CDOCKER interaction energy were calculated using the CDOCKER molecular docking algorithm in the Discovery Studio Client – Structure-Based Design software (Dassault Systemes BIOVIA, USA)

anti-aggregation activity was also confirmed by TEM studies which showed a reduction in the formation of Aβ42 fibrils. Strikingly, these benzamide derivatives demonstrated excellent neuroprotection against Aβ42-induced cytotoxicity in HT22 mouse hippocampal neuronal cells (80–97% cell viability at 25 µM) and were not toxic. Quantification of the Aβ42 fibril load in the ProteoStat-based live cell imaging confirmed the ability of compounds **3a, 5a**, and **7a** to reduce Aβ42 fibril load in the cellular environment (27–29% inhibition at 25 µM). In addition, these compounds were also able to offer neuroprotection to HT22 cells exposed to Aβ42 in the LDH assay.

These studies suggest that benzamide derivatives can bind to Aβ42 assemblies and have the potential to induce changes in their conformation and reduce their cytotoxic effects in the cellular environment. They also exhibit drug-like properties and do not possess any structural alerts, unlike the chalcone template that possesses the reactive α,β-unsaturated system which is considered as PAINS [25, 30]. Our studies show that benzamides possessing *N*-benzylbenzamide, *N*-phenethylbenzamide or *N*-benzyloxybenzamide templates, hold promise in the design and development of novel small molecules as Aβ42 aggregation inhibitors.

Experimental

General

All chemicals and reagents were purchased from various vendors (Sigma Aldrich USA, Alfa Aesar USA, Bio Basic Canada, AA Blocks USA, Cayman Chemical USA, Thermo Fisher USA, and Corning USA), were > 95% pure and used without further purification. The Aβ42 1,1,3,3,3-hexafluoroisopropanol (HFIP) > 95% pure, was purchased from Anaspec USA and rPeptide USA. The chemical reactions were monitored by thin-layer chromatography (TLC), Merck silica gel 60, F254. Column chromatography was carried out using Merck silica gel 230-400 mesh. The spots were visualized with short or long wavelengths (254 nm or 365 nm). The melting points of compounds were determined using a digital melting point apparatus (REACH Devices, USA). The proton NMR (^{1}H NMR) spectra of compounds were obtained using a 300 MHz Bruker Avance spectrometer. Either $CDCl_3$ or DMSO-d_6 were used as the solvents. Coupling constants (J values) were recorded in Hertz (Hz). Abbreviations used to represent ^{1}H NMR signals were s – singlet, d – doublet, t – triplet, m – multiplet, br s – broad singlet. The mass and purity were confirmed on Agilent 1260 Infinity liquid chromatography (LC) module equipped with 6130 Quadrupole mass spectrometry (Agilent 6100 series LCMS). The column used on LCMS was ZORBAX Eclipse AAA, 4.6 × 75 mm, 3.5 micron (Agilent Technologies, Canada). A mixture of water and acetonitrile 1:1 v/v with 0.1% formic acid (1.0 mL/min flow rate), was used as the solvent system to assess compound purity and

mass. The compounds were of ≥ 95% pure as determined by LCMS analysis before testing in various biological screening assays.

General procedure for the synthesis of 3a-h, 5a-h and 7a-h

Phenylmethanamine (**2**) (1 mmol), or 2-phenylethan-1-amine (**4**) (1 mmol), or *O*-benzylhydroxylamine (**6**) (1 mmol) was added into a 50 ml round bottom flask containing 15 ml anhydrous tetrahydrofuran (THF). To this mixture, 1.2 equivalent of triethylamine (TEA) and 1.0 equivalent of corresponding acid chlorides with various R groups were added (Scheme 1). The reaction was kept at either room temperature or under reflux for 6–24 h and monitored by TLC. After the reaction was complete, the solvent was evaporated in vacuo and the resulting reaction mixture was dissolved in 15 mL ethyl acetate (EtOAc), and then washed s with 15 mL brine solution (x 3). The organic layer was collected and dried over anhydrous $MgSO_4$ and filtered. The organic solvent was removed in vacuo and the residue/oil obtained was further purified by silica gel column chromatography using a combination of solvent systems (1:1 *n*-hexanes: EtOAc or 5:2 *n*-hexanes: EtOAc or 9:1 dichloromethane (DCM): Methanol (MeOH) or 4:1 DCM: *n*-hexanes) to afford the final compounds **3a–h, 5a–h** and **7a–h**. The yields ranged from 72–93%. The analytical data for these compounds are given in the following section. The ^{1}H NMR spectra and LCMS chromatograms are provided in the Supplementary Material document.

N-Benzylbenzamide (**3a**): White solid, 92.8% [40, 41]. ^{1}H NMR (300 MHz, DMSO-d_6) δ 9.00 (t, $J = 5.6$ Hz, 1H), 7.90–7.81 (m, 2H), 7.53–7.39 (m, 3H), 7.29–7.10 (m, 5H), 4.45 (d, $J = 6.0$ Hz, 2H). mp: 105–107 °C. ESI-MS, m/z for $C_{14}H_{14}NO$ $[M + H]^+$ 212.1. Purity: 99.9% (LCMS).

N-Benzylisonicotinamide (**3b**): White solid, 72% [41, 42]. ^{1}H NMR (300 MHz, DMSO-d_6) δ 9.33 (t, $J = 5.3$ Hz, 1H), 8.79–8.67 (m, 2H), 7.85–7.75 (m, 2H), 7.34–7.27 (m, 5H), 4.51 (d, $J = 6.0$ Hz, 2H). mp: 95–98 °C. ESI-MS, m/z for $C_{13}H_{13}N_2O$ $[M + H]^+$ 213.1. Purity: 99.0% (LCMS).

N-Benzylpicolinamide (**3c**): White solid, 74.3% [42]. ^{1}H NMR (300 MHz, DMSO-d_6) δ 9.32 (br s, 1H), 8.67–8.65 (m, 1H), 8.10–7.96 (m, 2H), 7.64–7.59 (m,1H), 7.35– 7.20 (m, 5H), 4.50 (d, $J = 6.4$ Hz, 2H). mp: 94–97 °C. ESI-MS, m/z for $C_{13}H_{13}N_2O$ $[M + H]^+$ 213.1. Purity: 99.6% (LCMS).

N-Benzyl-1*H*-pyrrole-2-carboxamide (**3d**): White solid, 79.6% [43]. ^{1}H NMR (300 MHz, $CDCl_3$) δ 9.50 (br s, 1H), 7.51–7.12 (m, 5H), 6.92–6.90 (m, 1H), 6.53–6.51 (m, 1H), 6.23–6.20 (m, 1H), 6.13 (br s, 1H), 4.60 (d, $J = 5.9$ Hz, 2H). mp:122–125 °C. ESI-MS, m/z for $C_{12}H_{13}N_2O$ $[M + H]^+$ 201.1. Purity: 96.1% (LCMS).

N-Benzylfuran-2-carboxamide (**3e**): White solid, 93% [44]. ^{1}H NMR (300 MHz, DMSO-d_6) δ 9.04 (t, $J = 5.8$ Hz, 1H), 7.84 (d, $J = 3.7$ Hz, 1H), 7.36–7.21 (m, 5H), 7.25 (d, $J = 6.0$ Hz, 1H), 6.62 (d, $J = 5.0$ Hz, 1H), 4.46 (d, $J = 6.0$ Hz, 2H). mp: 120–123 °C. ESI-MS, m/z for $C_{12}H_{12}NO_2$ $[M + H]^+$ 202.1. Purity: 99.6% (LCMS).

N-Benzylthiophene-2-carboxamide (**3 f**): White solid, 78.7% [42]. ^{1}H NMR (300 MHz, DMSO-d_6) δ 9.04 (t, $J = 5.7$ Hz, 1H), 7.88–7.81 (m, 1H), 7.39–7.19 (m, 5H), 7.15–7.05 (m, 2H), 4.45 (d, $J = 6.2$ Hz, 2H). mp: 115–117 °C. ESI-MS, m/z for $C_{12}H_{12}NOS$ $[M + H]^+$ 218.1. Purity: 99.7% (LCMS).

N-Benzyl-1-naphthamide (**3 g**): White solid, 87.6% [45]. ^{1}H NMR (300 MHz, DMSO-d_6) δ 9.09 (t, $J = 5.7$ Hz, 1H), 8.22–8.19 (m, 1H), 8.06–7.95 (m, 2H), 7.66–7.53 (m, 4H), 7.38–7.26 (m, 5H), 4.55 (d, $J = 6.2$ Hz, 2H). mp: 127–129 °C. ESI-MS, m/z for $C_{18}H_{16}NO$ $[M + H]^+$ 262.1. Purity: 98.3% (LCMS).

N-Benzylquinoline-2-carboxamide (**3 h**): White solid, 93.6% [46]. ^{1}H NMR (300 MHz, DMSO-d_6) δ 9.47 (t, $J = 6.2$ Hz, 1H), 8.58 (d, $J = 8.5$ Hz, 1H), 8.20–8.04 (m, 3H), 7.88 (t, $J = 7.6$ Hz, 1H), 7.73 (t, $J = 7.5$ Hz, 1H), 7.40–7.22 (m, 5H), 4.58 (d, $J = 6.2$ Hz, 2H). mp: 128–130 °C. ESI-MS, m/z for $C_{17}H_{15}N_2O$ $[M + H]^+$ 263.1. Purity: 99.5% (LCMS).

N-Phenethylbenzamide (**5a**): White solid, [47]. ^{1}H NMR (300 MHz, $CDCl_3$) δ 7.78–7.59 (m, 2H), 7.52–7.28 (m, 5H), 7.24 (q, $J = 4.9$, 4.4 Hz, 3H), 6.10 (s, 1H), 3.71 (q, $J = 6.9$ Hz, 2H), 2.93 (t, $J = 6.9$ Hz, 2H). mp: 122–125 °C. ESI-MS, m/z for $C_{15}H_{16}NO$ $[M + H]^+$ 226.1. Purity: 99.9% (LCMS).

N-Phenethylisonicotinamide (**5b**): White solid, 76% [42]. ^{1}H NMR (300 MHz, $CDCl_3$) δ 8.71–8.68 (m, 2H), 7.50–7.48 (m, 2H), 7.36–7.20 (m, 5H), 6.15 (br s, 1H), 3.72 (q, $J = 6.6$ Hz, 2H), 2.93 (t, $J = 6.8$ Hz, 2H). mp: 129-130 °C. ESI-MS, m/z for $C_{14}H_{15}N_2O$ $[M + H]^+$ 227.1. Purity: 98.7% (LCMS).

N-Phenethylpicolinamide (**5c**): Yellowish oil, 74.5% [48]. ^{1}H NMR (300 MHz, $CDCl_3$) δ 8.53 (d, $J = 4.5$ Hz, 1H), 8.22 (d, $J = 7.8$ Hz, 1H), 8.16 (s, 1H), 7.85 (td, $J = 7.7$, 1.6 Hz, 1H), 7.44–7.23 (m, 6H), 3.72 (q, $J = 7.0$ Hz, 2H), 2.97 (t, $J = 7.3$ Hz, 2H). ESI-MS, m/z for $C_{14}H_{15}N_2O$ $[M + H]^+$ 227.1. Purity: 99.9% (LCMS).

N-Phenethyl-1*H*-pyrrole-2-carboxamide (**5d**): White solid, 82.8% [49]. ^{1}H NMR (300 MHz, $CDCl_3$) δ 9.38 (br s, 1H), 7.37–7.26 (m, 2H), 7.26–7.17 (m, 3H), 6.91–6.88 (m, 1H), 6.41–6.38 (m, 1H), 6.20–6.17 (m, 1H), 5.84 (br s, 1H), 3.66 (q, $J = 6.7$ Hz, 2H), 2.88 (t, $J = 6.9$ Hz, 2H). mp: 134–136 °C. ESI-MS, m/z for $C_{13}H_{15}N_2O$ $[M + H]^+$ 215.1. Purity: 98.6% (LCMS).

N-Phenethylfuran-2-carboxamide (**5e**): White solid, 75.5% [47]. ^{1}H NMR (300 MHz, $CDCl_3$) δ 7.38–7.20 (m, 5H), 7.08 (d, $J = 3.5$ Hz, 1H), 6.46–6.36 (m, 2H), 3.67 (q,

$J = 7.0$ Hz, 2H), 2.90 (t, $J = 7.0$ Hz, 2H). mp: 115–117 °C. ESI-MS, m/z for $C_{13}H_{14}NO_2$ $[M + H]^+$ 216.1. Purity: 99.7% (LCMS).

N-Phenethylthiophene-2-carboxamide (**5 f**): White solid, 73.2% [50]. ^{1}H NMR (300 MHz, $CDCl_3$) δ 7.41–7.18 (m, 7H), 7.08–7.01 (m, 1H), 6.00 (br s, 1H), 3.67 (q, $J = 7.0$ Hz, 2H), 2.90 (t, $J = 7.0$ Hz, 2H). mp: 116–119 °C. ESI-MS, m/z for $C_{13}H_{14}NOS$ $[M + H]^+$ 232.1. Purity: 99.8% (LCMS).

N-Phenethyl-1-naphthamide (**5 g**): White solid, 72.8% [47]. ^{1}H NMR (300 MHz, $CDCl_3$) δ 8.20–8.16 (m, 1H), 7.81–7.75 (m, 2H), 7.50–7.44 (m, 3H), 7.40–7.23 (m, 6H), 5.96 (br s, 1H), 3.82 (q, $J = 6.6$ Hz, 2H), 2.99 (t, $J = 6.8$ Hz, 2H). mp: 125–128 °C. ESI-MS, m/z for $C_{19}H_{18}NO$ $[M + H]^+$ 276.1. Purity: 99.2% (LCMS).

N-Phenethylquinoline-2-carboxamide (**5 h**): White solid, 79.9% [51]. ^{1}H NMR (300 MHz, $CDCl_3$) δ 8.36–8.27 (m, 1H), 8.30 (s, 2H), 8.04 (d, $J = 8.5$ Hz, 1H), 7.86 (dd, $J = 8.1$, 1.5 Hz, 1H), 7.74 (ddd, $J = 8.5$, 6.9, 1.5 Hz, 1H), 7.60 (dd, $J = 8.2$, 6.8 Hz, 1H), 7.36–7.19 (m, 5H), 3.78 (q, $J = 7.6$ Hz, 2H), 2.99 (t, $J = 7.3$ Hz, 2H). mp: 81–84 °C. ESI-MS, m/z for $C_{18}H_{17}N_2O$ $[M + H]^+$ 277.1. Purity: 99.56% (LCMS).

N-(Benzyloxy)benzamide (**7a**): White solid, 77.9% [33]. ^{1}H NMR (300 MHz, DMSO-d_6) δ 11.76 (s, 1H), 7.75 (d, $J = 7.6$ Hz, 2H), 7.55–7.32 (m, 8H), 4.93 (s, 2H). mp: 104–106 °C. ESI-MS, m/z for $C_{14}H_{14}NO_2$ $[M + H]^+$ 228.1. Purity: 99.6% (LCMS).

N-(Benzyloxy)isonicotinamide (**7b**): White solid, 86.1%. ^{1}H NMR (300 MHz, DMSO-d_6) δ 12.07 (br s, 1H), 8.72 (d, $J = 4.9$ Hz, 2H), 7.65 (d, $J = 5.3$ Hz, 2H), 7.43 (dd, $J = 19.5$, 6.8 Hz, 5H), 4.96 (s, 2H). mp: 117–120 °C. ESI-HRMS, m/z for $C_{13}H_{14}N_2O_2$ $[M + H]^+$ 229.0977, found 229.0966. Purity: 99.4% (LCMS).

N-(Benzyloxy)picolinamide (**7c**): Yellowish oil, 77.0% [52]. ^{1}H NMR (300 MHz, DMSO-d_6) δ 12.04 (s, 1H), 8.61 (d, $J = 4.7$ Hz, 1H), 8.00 (d, $J = 4.0$ Hz, 2H), 7.62–7.37 (m, 6H), 4.95 (s, 2H). ESI-MS, m/z for $C_{13}H_{13}N_2O_2$ $[M + H]^+$ 229.1. Purity: 99.7% (LCMS).

N-(Benzyloxy)-1*H*-pyrrole-2-carboxamide (**7d**): White solid, [53]. ^{1}H NMR (300 MHz, $CDCl_3$) δ 9.51 (br s, 1H), 7.39–7.24 (m, 5H), 6.91 (td, $J = 2.7$, 1.3 Hz, 1H), 6.52 (dd, $J = 3.8$, 2.5 Hz, 1H), 6.21 (dt, $J = 3.7$, 2.6 Hz, 1H), 6.13 (br s, 1H), 4.60 (d, $J = 5.9$ Hz, 2H). mp: 77–80 °C. ESI-MS, m/z for $C_{12}H_{13}N_2O_2$ $[M + H]^+$ 217.1. Purity: 96.5% (LCMS).

N-(Benzyloxy)furan-2-carboxamide (**7e**): White solid, 77.9% [54]. ^{1}H NMR (300 MHz, DMSO-d_6) δ 11.74 (s, 1H), 7.86 (s, 1H), 7.46–7.36 (m, 5H), 7.10 (d, $J = 4.3$ Hz, 1H), 6.63 (s, 1H), 4.90 (s, 2H). mp: 82–85 °C. ESI-MS, m/z for $C_{12}H_{12}NO_3$ $[M + H]^+$ 218.1. Purity: 99.9% (LCMS).

N-(Benzyloxy)thiophene-2-carboxamide (**7 f**): White solid, 92.9% [55]. ^{1}H NMR (300 MHz, DMSO-d_6) δ 11.79 (s, 1H), 7.83–7.81 (m, 1H), 7.65–7.62 (m, 1H), 7.46–7.34 (m, 5H), 7.15 (d, $J = 4.3$ Hz, 1H), 4.92 (s, 2H). mp: 103–106 °C. ESI-MS, m/z for $C_{12}H_{12}NO_2S$ $[M + H]^+$ 234.1. Purity: 98.7% (LCMS).

N-(Benzyloxy)-1-naphthamide (**7 g**): White solid, 72.1% [56]. ^{1}H NMR (300 MHz, $CDCl_3$) δ 8.30–8.21 (m, 2H), 7.90 (d, $J = 8.2$ Hz, 1H), 7.87–7.79 (m, 1H), 7.58–7.32 (m, 8H), 5.13 (s, 2H). mp: 132–135 °C. ESI-MS, m/z for $C_{18}H_{16}NO_2$ $[M + H]^+$ 278.1. Purity: 98.9% (LCMS).

N-(Benzyloxy)quinoline-2-carboxamide (**7 h**): White solid, 80.1% [57]. ^{1}H NMR (300 MHz, $CDCl_3$) δ 10.35 (s, 1H), 8.26 (dd, $J = 8.5$ 1.5 Hz, 2H), 8.02 (d, $J = 8.5$ Hz, 1H), 7.9 (dd, $J = 8.2$, 1.4 Hz, 1H), 7.74 (dd, $J = 8.5$, 6.9 Hz, 1H), 7.61 (dd, $J = 8.1$, 6.8 Hz, 1H), 7.52–7.49 (m, 2H), 7.41–7.38 (m, 2H), 5.11 (s, 2H). ESI-MS, m/z for $C_{17}H_{18}N_2O_2$ $[M + H]^+$ 279.1. Purity: 99.7% (LCMS).

General procedure for the synthesis of 3i, 5i, 7i

Phenylmethanamine (**2**) (1 mmol), or 2-phenylethylamine (**4**) (1 mmol), or *O*-benzyloxyamine (**6**) (1 mmol) was added into a 50 mL round bottom flask containing 15 mL anhydrous THF. Next, 1.0 equivalent 1*H*-indole-2-carboxylic acid, 1.2 equivalent EDC hydrochloride, 1.5 equiv 1-hydroxybenzotriazole (HOBt), and 2.2 equivalent TEA were added in sequence. The reaction was kept at room temperature overnight. The solvent was evaporated in vacuo and the resulting reaction mixture was dissolved in 15 ml EtOAc and washed with 15 ml brine solution (x 3). The organic layer was collected, dried over anhydrous $MgSO_4$ and filtered. The organic solvent was then removed in vacuo to obtain a residue/oil which was further purified by silica gel column chromatography using either 1:1 *n*-hexanes: EtOAc or 5:2 *n*-hexanes: EtOAc as eluents to afford **3i, 5i** and **7i** in yields ranging from 80–92%. Their analytical data is given below. The ^{1}H NMR spectra and LCMS chromatograms are provided in the Supporting Information.

N-Benzyl-1*H*-indole-2-carboxamide (**3i**): White solid, 90.6% [45]. ^{1}H NMR (300 MHz, DMSO-d_6) δ 11.56 (s, 1H), 9.00 (t, $J = 6.1$ Hz, 1H), 7.57 (d, $J = 8.0$ Hz, 1H), 7.41 (d, $J = 8.2$ Hz, 1H), 7.38–7.27 (m, 4H), 7.17–7.12 (m, 3H), 7.03–6.98 (m, 1H), 4.49 (d, $J = 6.0$ Hz, 2H). mp: 229–232 °C. ESI-MS, m/z for $C_{16}H_{15}N_2O$ $[M + H]^+$ 251.1.Purity: 95.4% (LCMS).

N-(Phenethyl)-1*H*-indole-2-carboxamide (**5i**): White solid, 87.5% [58]. ^{1}H NMR (300 MHz, DMSO-d_6) δ 11.51 (br s, 1H), 8.57 (t, $J = 5.6$ Hz, 1H), 7.60 (d, $J = 7.9$ Hz, 1H), 7.43 (d, $J = 8.2$ Hz, 1H), 7.34–7.01 (m, 6H), 3.49–3.55 (m, 2H), 2.87 (t, $J = 7.4$ Hz, 2H). mp: 191–194 °C. ESI-MS, m/z for $C_{17}H_{17}N_2O$ $[M + H]^+$ 265.1. Purity: 97.6% (LCMS).

N-(Benzyloxy)-1*H*-indole-2-carboxamide (**7i**): White solid, 82.7% [59]. ^{1}H NMR (300 MHz, DMSO-d_6) δ 11.81 (s, 1H), 11.66 (s, 1H), 7.60 (d, $J = 7.9$ Hz, 1H), 7.42 (dq, $J = 14.0$, 7.0, 6.4 Hz, 6H), 7.20 (t, $J = 7.5$ Hz, 1H),

7.09–6.96 (m, 2H), 4.96 (s, 2H). mp: 152–155 °C. ESI-MS, m/z for $C_{16}H_{15}N_2O_2$ $[M + H]^+$ 267.1. Purity: 95.6% (LCMS).

Biological activity assay

ThT-based Aβ42 aggregation inhibition assay

The ability of benzamide derivatives **3a–i, 5a–i** and **7a–i** to inhibit the Aβ42 aggregation was evaluated using the thioflavin T (ThT) based fluorescence kinetic assay [34]. A 15 µM ThT solution was prepared in ultra-pure-water (UPW) in 50 mM glycine buffer. The pH of the solution was adjusted to 7.4 with 50 mM sodium hydroxide solution. The aggregation assay was carried out using 215 mM sodium phosphate dibasic heptahydrate buffer prepared in UPW and the pH was adjusted to 7.4 by using 50 mM hydrochloric acid solution. The Aβ42•HFIP > 95% pure (Anaspec, USA) was treated with 1% ammonium hydroxide solution to afford 1 mg/mL stock solution. The stock solution was then vortexed and sonicated for 5 min before diluted to 50 µM working solution using the assay buffer. The stock solutions of test compounds **3a–i, 5a–i, 7a–i** and resveratrol (RVT), were prepared in assay buffer with DMSO as the solubilizing agent (final concentration per well was less than 2%). The 24 h aggregation kinetics assay was carried out using 384-well plates (Costar, black, clear-bottom), by adding 44 µL of ThT, 12 µL of assay buffer, 16 µL of Aβ42 solution (10 µM final well concentration), and 8 µL of test compound dilution (25 µM) into each well. The Aβ42 control wells contained ThT, Aβ42 solution and the assay buffer without any test compound. The plates were covered with a transparent plate cover and were incubated at 37 °C for 24 h with shaking at 300 cpm between readings for 30 s. The readings were taken every 10 min (bottom reading), with an excitation wavelength of 440 nm and an emission wavelength of 490 nm using the BioTek Synergy H1 microplate reader. Each sample was measured in triplicate readings and the results were obtained based on three independent experiments.

TEM studies to determine Aβ42 morphology

The TEM assay was carried out by first running the Aβ42 aggregation assay (as described above in the ThT assay) [34] by incubating test compounds **3a, 3f, 3h, 5a, 5f** and **7a** (25 µM each) with Aβ42 (10 µM) for 24 h at 37 °C. The TEM grids were prepared by aliquoting 20 µL each sample from the 384-well plate after the 24 h incubation period. These samples were loaded onto 400-mesh formvar-coated copper grid (Electron Microscopy Sciences, USA). The grids were air-dried overnight before washing with 40 µL of UPW for three times. After washing, the grids were further air-dried for another 4 h. Then, grids were stained with 20 µL 2% phosphotungstic acid solution for 30 s. The imaging studies were carried out using a Philips CM 10 TEM (Dept. of Biology, University of Waterloo) at 60 kV and the micrographs were obtained through 14-megapixel AMT camera at 60,000X magnification.

Aβ42-induced cytotoxicity assay in mouse hippocampal HT22 neuronal cell line

The cytotoxicity and neuroprotective effects of benzamide derivatives **3a, 3f, 3h, 5a, 5f** and **7a** toward HT22 cells was carried out by using the UV-based cell metabolism assay kit (cell counting kit 8, CCK-8, TargetMol, USA). The HT22 cells were cultured in DMEM/F12 1:1 with the addition of glutamate supplemented with 10% FBS and 1% penicillin and streptomycin at 37 °C in 5% CO_2. The cells were seeded at a density of 50,000 cells per 1 mL. After 24 h, the cells were treated with various compounds (25 µM) prepared in phosphate buffer pH 7.4 and DMSO (less than 2%) and incubated for 48 h. After that, the CCK-8 reagent was added to each well, and incubated for another 2 h, before measuring the UV absorbance at 450 nm as per the manufacturer's protocol. The neuroprotective effects of test compounds (25 µM) toward Aβ42-induced cytotoxicity was determined by treating the HT22 cells with 5 µM of Aβ42•HFIP (> 95%, rPeptide USA), and then incubating for 48 h at 37 °C [34]. The cell viability assay was determined by adding the CCK-8 reagent and incubating for another 2 h to measure the absorbance at 450 nm. The cell viability was calculated as average percent cell viability based on quadruplicate readings and based on three independent experiments.

Fluorescence live cell imaging in mouse hippocampal HT22 cell line

The Aβ42 used in the assay was purchased from Bachem Americas Inc, Torrance, CA, USA. The HT22 cells were cultured and treated as per Aβ42-induced cytotoxicity assay. After treatment, the cells were washed with PBS and then stained with ProteoStat® working solution (prepared according to the vendor's manual, ENZO Life Sciences, USA) for 20 min under dark at 37 °C [35]. Then the cells were washed with PBS three times with 5 min incubation at 37 °C to rinse out the excessive amount of dye. The cells were then visualized with an EVOS® FL Auto imaging system with an RFP light cube at fixed light intensity. The binary masks were generated by thresholding the original fluorescence images using the Huang algorithm in ImageJ software and used to measure the integrated gray value (IGV) of ProteoStat®-positive stains. The results presented

are averages of three independent experiments with three randomized views.

LDH release cytotoxicity assay in mouse hippocampal HT22 cell line

The CytoScan® LDH assay kit was used to determine the LDH release (G-Biosciences, St. Louis, MO, USA) [37]. The reagents and solutions were prepared according to vendor's manual. The HT22 cells were cultured and treated with 10 µM Aβ42 (Bachem, USA) as per Aβ42-induced cytotoxicity assay protocol. After treatment, 50 µL of the cell medium was transferred to a new well plate followed by the addition of 50 µL reaction mixture and further incubated for 20 min at 37 °C. This was followed by the addition of 50 µL stop solution before taking the readings at 490 nm and 680 nm. The percentage LDH release was calculated by subtracting the absorbance reading at 680 nm from that of 490 nm, and compared to Aβ42 control group. The results shown are averages of quadruplicate readings based on three independent experiments.

Molecular docking studies of compounds in Aβ42

The binding interactions **3a** (*N*-benzylbenzamide), **5a** (*N*-phenethylbenzamide) and **7a** (*N*-benzyloxybenzamide) Aβ42 were investigated by carrying out molecular docking studies conducted on Discovery Studio software program v20.1.0.19295, Structure-Based-Design program (BIOIA Inc. San Diego, USA). The Aβ42 pentamer model was prepared by extracting the coordinates from the solved 3D structure of Aβ42 fibril (PDB id: 5KK3) [34, 39]. A binding sphere of 20 Å radius was selected and defined as the ligand binding site which covers the KLVFFA and the C-terminal IGLMVGGVVIA hydrophobic region of the Aβ42. Compounds **3a, 5a** and **7a** were built in 3D using the *Small Molecules* module in the software and were subjected to energy minimization protocol (1000 and 2000 steps of steepest descent followed by conjugate gradient method) using CHARMm force field. The CDOCKER algorithm was used to carry out the docking studies. The *Receptor-Ligand Interactions* module in the software was used to perform CDOCKER simulations. The docking simulation included 2000 heating steps, a heating target temperature of 700 K and 5000 cooling steps and a cooling target temperature of 300 K. The top ligand binding modes of **3a, 5a** and **7a** with Aβ42 pentamer assembly was analyzed by evaluating the CDOCKER energy and CDOCKER interaction energies (in kcal/mol). Further analysis was carried out by determining the polar and nonpolar contacts of test compounds in the Aβ42 pentamer assembly.

In silico physicochemical and ADME analysis

The physicochemical properties including H-bond acceptors, H-bond donors, topological polar surface area (TPSA), blood-brain barrier permeability (BBB), lipophilicity parameter Log P, and structural alert flags were calculated for representative compounds (**3a, 3f, 5a, 7a** and chalcone) using the SwissADME web tool [38].

Supplementary information The online version contains supplementary material available at https://doi.org/10.1007/s00044-024-03256-6.

Acknowledgements The authors would like to thank the School of Pharmacy, University of Waterloo, NSERC-Discovery (RGPIN: 03830-2014 and 2020-05066), TD Pooler Charitable Foundation 2023-24, Canada Foundation for Innovation, CFI-JELF; Ontario Research Fund (ORF) and Early Researcher Award, Ministry of Research and Innovation, Government of Ontario, Canada (PR) for financial support of this research project.

Author contributions PPNR and YZ conceived the project and designed experiments. YZ, AS and AAF performed experiments. PPNR, YZ, AS and AAF analyzed and interpreted results. PPNR and YZ wrote the manuscript. PPNR, YZ, AS and AAF revised the manuscript.

Compliance with ethical standards

Conflict of interest The authors declare no competing interests.

References

1. Lyketsos CG, Carrillo MC, Ryan JM, Khachaturian AS, Trzepacz P, Amatneik J, Miller SM. Neuropsychiatric symptoms in Alzheimer's disease. Alzheimers Dement. 2011;7:532–9. https://doi.org/10.1016/J.JALZ.2011.05.2410
2. Atri A. The Alzheimer's disease clinical spectrum: diagnosis and management. Med Clin North Am. 2019;103:263–93. https://doi.org/10.1016/J.MCNA.2018.10.009
3. Porsteinsson AP, Isaacson RS, Knox S, Sabbagh MN, Rubino I. Diagnosis of early Alzheimer's disease: clinical practice in 2021. J Prev Alzheimers Dis. 2021;8:371–86. https://doi.org/10.14283/JPAD.2021.23
4. Knopman DS, Amieva H, Petersen RC, Chetelat G, Holtzman DM, Hyman BT, Jones DT. Alzheimer disease. Nat Rev Dis Primers. 2021;7:33. https://doi.org/10.1038/S41572-021-00269-Y
5. Selkoe DJ, Hardy J. The amyloid hypothesis of Alzheimer's disease at 25 years. EMBO Mol Med. 2016;8:595–608. https://doi.org/10.15252/EMMM.201606210
6. Kumar A, Singh A, Ekavali. A review on Alzheimer's disease pathophysiology and its management: An update. Pharmacol. Rep. 2015;67:195–203. https://doi.org/10.1016/j.pharep.2014.09.004
7. Deture MA, Dickson DW. The neuropathological diagnosis of Alzheimer's disease. Mol Neurodegener. 2019;14:32. https://doi.org/10.1186/S13024-019-0333-5
8. Kametani F, Hasegawa M. Reconsideration of amyloid hypothesis and tau hypothesis in Alzheimer's disease. Front Neurosci. 2018;12:25. https://doi.org/10.3389/FNINS.2018.00025
9. Aisen PS, Cummings J, Jack CR, Morris JC, Sperling R, Frolich L, Dubois B. On the path to 2025: understanding the Alzheimer's

disease continuum. Alzheimers Res Ther. 2017;9:60. https://doi.org/10.1186/S13195-017-0283-5
10. Zhang H, Ma Q, Zhang YW, Xu H. Proteolytic processing of Alzheimer's β-amyloid precursor protein. J Neurochem. 2012;120:9–21. https://doi.org/10.1111/J.1471-4159.2011.07519.X
11. Cummings J, Lee G, Nahed P, Kambar MEZN, Zhong K, Fonesca J, Taghva K Alzheimer's disease drug development pipeline: 2022. Alzheimers Dement. 2022;8:e12295. https://doi.org/10.1002/TRC2.12295
12. Cummings J, Lee G, Ritter A, Sabbagh M, Zhong K. 2020. Alzheimer's disease drug development pipeline: 2020. Alzheimers and Dement. 2020;6:e12050. https://doi.org/10.1002/trc2.12050
13. Sevigny J, Chiao P, Bussière T. The antibody aducanumab reduces Aβ plaques in Alzheimer's disease. Nature. 2016;537:50–56. https://doi.org/10.1038/nature19323
14. Salloway S, Chalkias S, Barkhof F, Barakos J, Purcell D, Suhy J, Smirnakis K. Amyloid-related imaging abnormalities in 2 Phase 3 studies evaluating aducanumab in patients with early Alzheimer disease. JAMA Neurol. 2022;79:13–21. https://doi.org/10.1001/JAMANEUROL.2021.4161
15. Van Dyck CH, Swanson CJ, Aisen P, Bateman RJ, Chen C, Gee M, Iwatsubo T. Lecanemab in early Alzheimer's disease. N Engl J Med. 2023;388:142–3. https://doi.org/10.1056/NEJMOA2212948
16. Reardon S. Alzheimer's drug donanemab: what promising trial means for treatments. Nature. 2023;617:232–3. https://doi.org/10.1038/D41586-023-01537-5
17. Makurvet FD. Biologics vs. small molecules: Drug costs and patient access. Med Drug Discov. 2021;9:100075. https://doi.org/10.1016/J.MEDIDD.2020.100075
18. Mohamed T, Yeung JCK, Vasefi MS, Beazely MA, Rao PPN. Development and evaluation of multifunctional agents for potential treatment of Alzheimer's disease: Application to a pyrimidine-2,4-diamine template. Bioorg Med Chem Lett. 2012;22:4707–12. https://doi.org/10.1016/j.bmcl.2012.05.077
19. Mohamed T, Shakeri A, Tin G, Rao PPN. Structure-activity relationship studies of isomeric 2,4-diaminoquinazolines on β-amyloid aggregation kinetics. ACS Med Chem Lett. 2016;7:502–7. https://doi.org/10.1021/acsmedchemlett.6b00039
20. Mohamed T, Shakeri A, Rao PPN. Amyloid cascade in Alzheimer's disease: recent advances in medicinal chemistry. Eur J Med Chem. 2016;113:258–72. https://doi.org/10.1016/J.EJMECH.2016.02.049
21. Sashidhara KV, Kumar M, Modukuri RK, Sonkar R, Bhatia G, Khanna AK, Shukla R. Synthesis and anti-inflammatory activity of novel biscoumarin–chalcone hybrids. Bioorg Med Chem Lett. 2011;21:4480–4. https://doi.org/10.1016/j.bmcl.2011.06.002
22. Kim MJ, Lee YH, Kwak J, Na Y, Yoon HG. Protective effects of a chalcone derivative against Aβ-induced oxidative stress and neuronal damage. BMB Rep. 2011;44:730–4. https://doi.org/10.5483/BMBREP.2011.44.11.730
23. Cao Z, Yang J, Xu R, Song Q, Zhang X, Liu H, Deng Y. Design, synthesis and evaluation of 4'-OH-flurbiprofen-chalcone hybrids as potential multifunctional agents for Alzheimer's disease treatment. Bioorg Med Chem. 2018;26:1102–15. https://doi.org/10.1016/J.BMC.2018.01.030
24. Liu HR, Liu XJ, Fan HQ, Tang JJ, Gao XH, Liu WK. Design, synthesis and pharmacological evaluation of chalcone derivatives as acetylcholinesterase inhibitors. Bioorg Med Chem. 2014;22:6124–33. https://doi.org/10.1016/J.BMC.2014.08.033
25. Jackson PA, Widen JC, Harki DA, Brummond KM. Covalent modifiers: a chemical perspective on the reactivity of α,β-unsaturated carbonyls with thiols via hetero-Michael addition reactions. J Med Chem. 2017;60:839–85. https://doi.org/10.1021/ACS.JMEDCHEM.6B00788
26. Zhuang C, Zhang W, Sheng C, Zhang W, Xing C, Miao Z. Chalcone: a privileged structure in medicinal chemistry. Chem Rev. 2017;117:762–7810. https://doi.org/10.1021/acs.chemrev.7b00020
27. Baell J, Walters MA. Chemistry: chemical con artists foil drug discovery. Nature. 2014;513:481–3. https://doi.org/10.1038/513481A
28. Baell JB. Redox-active nuisance screening compounds and their classification. Drug Discov Today. 2011;16:840–1. https://doi.org/10.1016/j.drudis.2011.06.011
29. Burgos-Morón E, Calderón-Montaño JM, Salvador J, Robles A, Lazaro ML. The dark side of curcumin. Int J Cancer. 2010;126:1771–5. https://doi.org/10.1002/IJC.24967
30. Baell JB, Holloway GA. New substructure filters for removal of pan assay interference compounds (PAINS) from screening libraries and for their exclusion in bioassays. J Med Chem. 2010;53:2719–40. https://doi.org/10.1021/JM901137J
31. Brahmachari S, Paul A, Segal D, Gazit E. Inhibition of amyloid oligomerization into different supramolecular architectures by small molecules: mechanistic insights and design rules. Future Med Chem. 2017;9:797–810. https://doi.org/10.4155/FMC-2017-0026
32. Katritzky AR, Kirichenko N, Rogovoy BV Efficient conversions of carboxylic acids into *O*-alkyl, *N*-alkyl and *O,N*-dialkylhydroxamic acids. Synthesis 2003; 2777-80. https://doi.org/10.1055/S-2003-42488
33. Majewski MW, Cho S, Miller PA, Franzblau SG, Miller MJ. Syntheses and evaluation of substituted aromatic hydroxamates and hydroxamic acids that target Mycobacterium tuberculosis. Bioorg Med Chem Lett. 2015;25:4933–6. https://doi.org/10.1016/J.BMCL.2015.04.099
34. Gujral SS, Shakeri A, Hejazi L, Rao PPN. Design, synthesis and structure-activity relationship studies of 3-phenylpyrazino[1,2-a]indol-1(2*H*)-ones as amyloid aggregation and cholinesterase inhibitors with antioxidant activity. Eur J Med. Chem. Rep. 2022;6:100075. https://doi.org/10.1016/J.EJMCR.2022.100075
35. Navarro S, Carija A, Munoz-Torrero D, Ventura S. A fast and specific method to screen for intracellular amyloid inhibitors using bacterial model systems. Eur. J. Med. Chem. 2016;121:785–92. https://doi.org/10.1016/j.ejmech.2015.10.044
36. Sandler OP, Miller Y. Molecular mechanisms of membrane-associated amyloid aggregation: computational perspective and challenges. Biochem. Biophys. Acta. Biomembr. 2018;1860:1889–905. https://doi.org/10.1016/j.bbamem.2018.03.014
37. Kumar P, Nagarajan A, Uchil PD Cold Spring Harb. Protoc. 2018; 2018. https://doi.org/10.1101/pdb.prot095497
38. Daina A, Michielin O, Zoete V. SwissADME: a free web tool to evaluate pharmacokinetics, drug-likeness and medicinal chemistry friendliness of small molecules. Sci Rep. 2017;7:42717. https://doi.org/10.1038/SREP42717
39. Colvin MT, Silvers R, Ni QZ, Can TV, Sergeyev I, Rosay M, Griffin RG. Atomic resolution structure of monomorphic Aβ42 amyloid fibrils. J Am Chem Soc. 2016;138:9663–74. https://doi.org/10.1021/JACS.6B05129
40. Ojeda-Porras A, Santana AH, Sanchez DG. Direct amidation of carboxylic acids with amines under microwave irradiation using silica gel as a solid support. Green Chem. 2015;17:3157–63. https://doi.org/10.1039/C5GC00189G
41. Li Y, Chen H, Liu J, Wan X, Xu Q. Clean synthesis of primary to tertiary carboxamides by CsOH-catalyzed aminolysis of nitriles in water. Green Chem. 2016;18:4865–70. https://doi.org/10.1039/C6GC01565D
42. Laha JK, Gulati U, Gupta A. Decarboxylative amidation of aryl/heteroarylacetic acids via activated esters through traceless α-functionalized benzylic radicals. Org Lett. 2023;25:3402–6. https://doi.org/10.1021/ACS.ORGLETT.3C00927

43. Darnowski MG, Lanosky TD, Paquette AR, Boddy CN. Synthesis of a constitutional Isomer of armeniaspirol A, pseudoarmeniaspirol A, via Lewis acid-mediated rearrangement. J Org Chem. 2022;87:15634–43. https://doi.org/10.1021/ACS.JOC.2C02331
44. Hamstra DFJ, Lenstra DC, Koenders TJ, Rutjes PJT, Mecinovic J. Poly(methylhydrosiloxane) as a green reducing agent in organophosphorus-catalysed amide bond formation. Org Biomol Chem. 2017;15:6426–32. https://doi.org/10.1039/C7OB01510K
45. Das J, Banerjee D. Nickel-catalyzed phosphine free direct *N*-alkylation of amides with alcohols. J Org Chem. 2018;83:3378–84. https://doi.org/10.1021/acs.joc.7b03215
46. Ren W, Yamane M. Mo(CO)(6)-mediated carbamoylation of aryl halides. J Org Chem. 2010;75:8410–5. https://doi.org/10.1021/JO101611G
47. Dumas AM, Molander GA, Bode JW. Amide-forming ligation of acyltrifluoroborates and hydroxyamines in water. Angew Chem Int Ed Engl. 2012;51:5683–6. https://doi.org/10.1002/anie.201201077
48. Xu S, Jiang D, Peng Z, Hu L, Liu T, Zhao L, Zhao J. Ynamide-mediated peptide bond formation: Mechanistic study and synthetic applications. Angew Chem Int Ed Engl. 2022;61:e202212247. https://doi.org/10.1002/ANIE.202212247
49. Dyson L, Wright AD, Young KA, Sakoff JA, McCluskey A. Synthesis and anticancer activity of focused compound libraries from the natural product lead, oroidin. Bioorg Med Chem. 2014;22:1690–9. https://doi.org/10.1016/J.BMC.2014.01.021
50. Fu R, Yang Y, Zhang J, Shao J, Xia X, Ma Y, Yuan R. Direct oxidative amidation of aldehydes with amines catalyzed by heteropolyanion-based ionic liquids under solvent-free conditions via a dual-catalysis process. Org Biomol Chem. 2016;14:1784–93. https://doi.org/10.1039/C5OB02376A
51. Gonec T, Bobal P, Sujan J, Pesko M, Guo J, Kralova K, Jampile J. Investigating the spectrum of biological activity of substituted quinoline-2-carboxamides and their isosteres. Molecules. 2012;17:613–44. https://doi.org/10.3390/MOLECULES17010613
52. Chen X, Han J, Zhu Y, Yuan C, Zhang J, Zhao Y. Transformation of masked benzyl alcohols to o-aminobenzaldehydes through C-H activation: a facile approach to quinazolines. Chem Commun. 2016;52:10241–4. https://doi.org/10.1039/C6CC05560E
53. Huang M, Hou J, Yang R, Zhang L, Zhu X, Wan W. A catalyst system, copper/*N*-methoxy-1*H*-pyrrole-2-carboxamide, for the synthesis of phenothiazines in poly(ethylene glycol). Synthesis. 2014;46:3356–64. https://doi.org/10.1055/S-0034-1379045
54. Kurz T, Pein MK, Marek L, Behrendt CT, Spanier L, Kuna K, Brucher K Microwave-assisted conversion of 4-nitrophenyl esters into 0-protected hydroxamic acids. Eur J Org Chem. 2009; 2939-42. https://doi.org/10.1002/EJOC.200900201
55. Sharma N, Saha R, Parveen N, Sekar G. Palladium-nanoparticles-catalyzed oxidative annulation of benzamides with alkynes for the synthesis of isoquinolones. Adv Synth Catal. 2017;359:1947–58. https://doi.org/10.1002/ADSC.201601137
56. Moutanea OG, Mantzourani C, Kokotou MG, Kokotos CG, Kokotos G. Sunlight- or UVA-light-mediated synthesis of hydroxamic acids from carboxylic acids. Eur. J. Org. Chem. 2023;26:e202300046. https://doi.org/10.1002/ejoc.202300046
57. Paolino M, Brindisi M, Vallone A, Butini S, Campiani G, Nannicini C, Brogi S. Development of potent inhibitors of the mycobacterium tuberculosis virulence factor Zmp1 and evaluation of their effect on mycobacterial survival inside macrophages. ChemMedChem. 2018;13:422–30. https://doi.org/10.1002/CMDC.201700759
58. Xu X, Feng H, Huang L, Liu X. Direct amidation of carboxylic acids through an active α-acyl enol ester intermediate. J. Org Chem. 2018;83:7962–9. https://doi.org/10.1021/ACS.JOC.8B00819
59. Schlegel M, Schneider C. Iron(III)-catalyzed (4 + 2)-cycloannulation of 2-hydroxy ketoxime ethers with indol-2-ylamides: synthesis of indole-fused 2-piperidinones. J Org Chem. 2019;84:5886–92. https://doi.org/10.1021/ACS.JOC.9B00261

Publisher's note Springer Nature remains neutral with regard to jurisdictional claims in published maps and institutional affiliations.

Springer Nature or its licensor (e.g. a society or other partner) holds exclusive rights to this article under a publishing agreement with the author(s) or other rightsholder(s); author self-archiving of the accepted manuscript version of this article is solely governed by the terms of such publishing agreement and applicable law.